

58(1), pp. 37-45, 2014

DOI: [10.3311/PPme.7392](https://doi.org/10.3311/PPme.7392)

Creative Commons Attribution 

Ádám Ugron, György Paál

RESEARCH ARTICLE

RECEIVED 29 SEPTEMBER 2013; ACCEPTED 18 JANUARY 2014

## Abstract

*Cerebral aneurysms are bulges appearing on brain arteries. The development, growth and rupture has been intensively studied using numerical tools. We present a series of studies covering many of the open questions related to the boundary conditions used in numerical simulations, namely the inlet, outlet and the wall. The effect of boundary conditions cannot be overestimated; yet it received much less attention than it would have deserved.*

*An analytical formula of the pulsating pipe flow with rigid walls is used to study the effects of the varying parameters of the cardiac cycle. Both idealised and real geometries are used to study the propagation of the boundary effects, and to analyse the effects of distensible boundaries.*

*Our results provide useful criteria for the necessary inlet and outlet length. We found that the deformability of wall boundaries has a significant influence; however, simulations with rigid walls are still able to capture the main hemodynamic properties of the flow.*

*The results can be effectively used in the simulation of cerebral aneurysm and provide a firmer ground in a broader sense for hemodynamic simulations.*

## Keywords

*hemodynamics · cerebral aneurysm · boundary condition · Womersley · fluid-structure interaction*

## Ádám Ugron

Department of Hydrodynamic Systems,  
Budapest University of Technology and Economics  
P.o. Box 91., H-1521 Budapest, Hungary  
e-mail: [ugron@hds.bme.hu](mailto:ugron@hds.bme.hu)

## György Paál

Department of Hydrodynamic Systems,  
Budapest University of Technology and Economics  
P.o. Box 91., H-1521 Budapest, Hungary  
e-mail: [paal@hds.bme.hu](mailto:paal@hds.bme.hu)

## 1 Introduction

Aneurysms are dilated sections of blood vessels appearing at various locations of the cardiovascular system. These lesions may appear on the arteries supplying the brain, the cerebral circulation. Aneurysms that rupture on the cerebral arteries cause subarachnoid haemorrhage, a form of stroke, which may lead to the death or permanent disability of the patient. Studies show [1] that approximately 5% of the population develops an aneurysm, but only a fraction of these burst. Unfortunately the knowledge about the initiation, growth and rupture of cerebral aneurysms is limited even though research on the field is intense.

It is a widely accepted view that hemodynamics is a key factor in these processes [2]. The studies whose aim is to understand the hemodynamics of cerebral aneurysms are most commonly based on numerical simulations. The flow inside vessels are usually assumed to be laminar, blood is treated as an incompressible, Newtonian liquid. With these assumptions advanced numerical solvers are able to calculate the flow accurately. The uncertainties of the results therefore mostly originate from the geometry, meshing and boundary conditions.

Once a patient-specific image is acquired, the effect of slight geometrical uncertainties arising from reconstruction are found to be less dominant. Cebra et al. [3] found the calculated flow to be insensitive to slight geometrical variations. They compared results based on models derived from the same medical images by different persons. With the exception of one case, they found small differences. There the parent artery and the sac touched each other. The small geometrical uncertainties are the results of the image segmentation as it is based on the medical imaging technique. This in itself holds numerous uncertainties, which are beyond the scope of the present paper.

Meshing is also a less critical factor. Advanced mesh generation codes that are part of numerical simulation packages are able to generate high quality meshes. These include the appropriate resolution near the vessel wall, which can be efficiently assured using prismatic elements. The effect of these grids on numerical accuracy can be well monitored with the help of mesh studies.

To control uncertainties introduced by boundary conditions is a key to accurate results. Cerebral circulation, being an internal flow, has three types of boundary conditions: the inlet, and outlet boundary and the wall. The current paper focuses on these.

At the inlet boundary usually a measured history of the mean velocity in the cardiac cycle is prescribed [4,5]. Ideally, these measured signals are available in each patient-specific case. If this is not the case either a previously measured signal or an artificial approximation is used [6]. Spatially, the flow profile is assumed to be the Poiseuille solution [6] or the analytic solution for periodic pulsatile flow, the Womersley profile [3]. Some proposed a multi-scale approach to address the problem of boundary condition definition. Formaggia et al. [7] couples a one-dimensional (1D) pipe network model to the three dimensional (3D) computational domain to obtain boundary conditions. This can be applied to both in- and outlet boundaries.

For the outlet boundary there are several additional methods in the literature. Apart from prescribing measured or artificial pressure histories or even setting the outlet pressure to a constant level, there are the so-called vascular bed approaches [8]. These are based on the fact that on the level of capillaries an almost constant pressure is present [9]. Therefore, after modelling the intermediate vascular tree, prescribing the proper pressure values on the boundary is relatively easy. The vascular bed may be modelled with series of parallel resistors, as a fractal tree or with a porous medium [10] as it is in the present case. There are additional approaches like modelling the vascular tree with 0D (lumped) or 1D methods and coupling it to the 3D simulations. Grinberg and Karniadakis [11] summarise the various approaches in detail.

The vessel wall is in most cases treated as rigid ignoring its distensibility, because the latter would be computationally intensive to include in a model. This assumption may limit the accuracy, as it was shown by Torii et al. [12] that it has a significant effect on the wall shear stress (WSS) distribution on the vessel.

Some authors investigated the sensitivity of the flow on several boundary conditions [3,5,13]. They concluded that the flow is most sensitive to the temporal history of the flow rate. The influence of the upstream parent artery geometry was also found to be important [14].

The current paper studies the assumptions of the boundary conditions in terms of flow and geometry. The inlet conditions are investigated by studying the upstream conditions of the aneurysm sac. Entrance length and pulsatility features are investigated with the help of various vessel geometries. Some findings of the outlet boundary with the applied methodology are discussed. The effects of compliant walls are also studied briefly and some results are presented in the paper.

## 2 Methods

Our study simulates the fluid dynamic processes in cerebral aneurysms with the help of Computational Fluid Dynamics (CFD).

### 2.1 Applied software

The applied CFD code was the commercially available ANSYS CFX, whereas the Finite Element Method (FEM) code was ANSYS. For meshing, ANSYS ICEM CFD was used. Fluid-Structure Interaction (FSI) simulations are performed using the ANSYS software environment. MATLAB and ParaView were used for some additional calculations and post-processing.

### 2.2 Computational models

Incompressible, laminar flow was assumed. The fluid is treated as Newtonian with a density of  $\rho = 1050 \text{ kg/m}^3$  and a viscosity of  $\mu = 0.003 \text{ Pa s}$ . For the compliant studies the vessel wall material was assumed to be linearly elastic with an elasticity modulus of  $E = 1 \text{ MPa}$  and a Poisson ratio of  $\nu = 0.35$ . The linearly elastic approach is a reasonable assumption in case of the arteries of the brain. Here the stiffening effect of the wall material is not apparent in the usual load range because of the small deformation rate [12].

For inlet length studies a simple straight tube was considered as the flow domain. Its diameter was  $d = 3 \text{ mm}$  and the length was  $60d$ . The mesh had a fine resolution near the wall to calculate high velocity gradients accurately. The block-structured hexahedral O-grid mesh of the geometry was made of approximately 800,000 elements, which enabled us to capture the velocity profile development along the longitudinal axis. Two additional geometries were used in several simulations. An idealised side-wall aneurysm in a bend and a bifurcation aneurysm (Fig. 1) were used to capture the most essential properties of cerebral aneurysms.

These two models were used in studies on entrance and exit length as well as in wall compliance studies. They had tetrahedral core meshes; the *a* and *b* configurations consisted of approximately 120,000 and 220,000 elements, respectively. Prism elements were used in the vicinity of the wall. The actual mesh size varied from case to case due to the different entrance and exit lengths attached to the core mesh. In the compliant cases the finite element mesh, modelling the vessel wall, was built up using 4 node tetrahedral finite elements by prescribing  $s = 0.4 \text{ mm}$  uniform wall thickness. Both FEM meshes belonging to the artificial aneurysms consisted of approximately 30,000 nodes.

Two real aneurysm models were also studied; a side-wall aneurysm and a bifurcation aneurysm. The 3D data of these were acquired using standard medical imaging (rotational digital subtraction angiography). These data are transformed and processed by ParaView. Here surfaces of the aneurysm geometries were generated based on constant intensity level surfaces of the images. These raw surfaces are slightly smoothed using a Laplacian smoothing algorithm, the small vessels are removed and the feeding and exiting vessels are cut, additionally the holes of the surface are covered. Tetrahedral meshes were generated inside these surfaces with 5 layers of prismatic cells near the walls. The tetrahedral CFD meshes consisted of 530,000 and 390,000 elements in case of the side-wall and the bifurcation aneurysm, respectively. Four-node shell elements

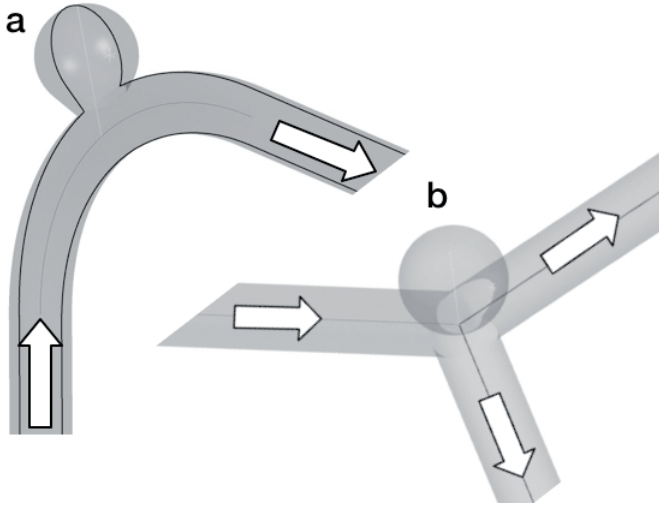


Fig. 1. Aneurysm models and flow directions for boundary condition studies, side-wall aneurysm in a bend (a) and bifurcation aneurysm (b)

were created on the surface of the geometry for solid body simulation with 17,000 (side-wall) and 13,000 (bifurcation) nodes.

The complete vessel geometry obtained from rotational angiography has to be cut to a finite length for the purposes of the simulations, therefore, it has to be decided how much of the parent vessel can be removed without jeopardising accuracy. To study the effect of the neglected inlet vessel section, curved pipes were generated. The diameter of these sections was a constant  $d = 3$  mm, the length varied between 100 - 150d. The meshes were extruded hexagonal O-grid meshes. As a result of a mesh study the computational volume consisted of 420,000 elements in all cases, one cross section consisted of 420 surface elements. Additionally, a third real aneurysm geometry was prepared for simulation that had a sufficiently long inlet vessel section. The base mesh of the geometry without the inlet section consisted of 630,000 elements.

Unsteady simulations were carried out with a time step  $t = 0.01$  s except the two real aneurysms used in compliancy studies in which case  $t = 0.02$  s was applied in the coupled and the rigid-walled simulations. The simulation duration varied between 2 - 4 cardiac cycles. The period time of the cycles was  $T = 0.8$  s, therefore, the length of the simulations varied between 1.6 s - 3.2 s depending on the sensitivity of the problem. The applied numerical schemes were of second order both in time and space.

### 2.3 Inlet conditions

The main idea of the inlet studies was to discover the error sources of the boundary condition prescriptions and determine whether these errors reach the location of interest or not. To this end, velocity profiles were studied first in the case of straight blood vessels, then the development of profiles with changing inlet length of the tubes. In the case of curved tubes the two steps were done simultaneously.

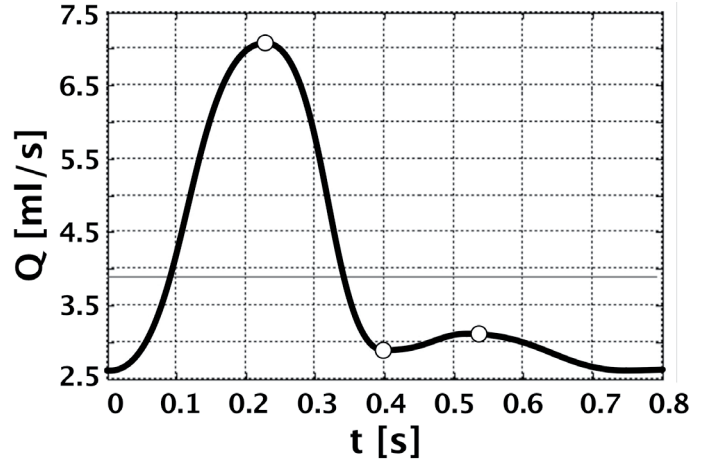


Fig. 2. Idealised cardiac cycle used in most studies with the characteristic points marked, the average flow rate is denoted with the thin grey line

#### 2.3.1 Adaptation of the Womersley formula

The Womersley formula gives an analytical solution for the temporal and spatial velocity distribution in case of periodically pulsating laminar flow in a cylindrical pipe with rigid walls [15]. Based on the solution, the relation between the periodic flow rate and the velocity distribution can be given in the form of a Fourier series (Eq. (1) and (2)) [3].

$$u(r,t) = \frac{2Q_0}{\pi R^2} \left[ 1 - \left( \frac{r}{R} \right)^2 \right] + \sum_{n=1}^N \frac{Q_n}{\pi R^2} \frac{1 - \frac{J_0\left(\beta_n \frac{r}{R}\right)}{J_0(\beta_n)}}{1 - \frac{2J_1(\beta_n)}{\beta_n J_0(\beta_n)}} e^{in\omega t} \quad (1)$$

where

$$\beta_n = i^{\frac{3}{2}} \alpha_n = i^{\frac{3}{2}} R \sqrt{\frac{n\omega}{\nu}} \quad (2)$$

Here  $u$  is the axial velocity,  $r$  is the distance inside the pipe from the centre,  $t$  is the time.  $Q$  is the volume flow rate,  $R$  is the radius of the pipe.  $J_0$  and  $J_1$  are the zeroth and first order Bessel functions of the first kind,  $\nu$  is the kinematic viscosity,  $\omega$  is the frequency,  $\alpha$  is the Womersley number and  $i$  is the imaginary unit. Additionally,  $n$ , the subscript of  $Q$  denotes the number of the harmonic component of the Fourier decomposed cardiac cycle.

The reconstruction of velocity profiles was implemented in the MATLAB environment. A parametrized cardiac cycle was created which was able to capture the basic properties of a real cardiac cycle such as frequency and mean value. The location of characteristic points like the systolic maximum or diastolic minimum flow rate were also parametrised and denoted by empty circles in Fig. 2.

The generated cardiac cycle was expanded into Fourier series using an algorithm based on MATLAB's built-in Fast Fourier Transform (FFT) routine, thereby calculating the  $Q_n$ -s in Eq. (1). The Womersley profile was then approximately generated using the first 10 Fourier components in Eq. (1). These Womersley profiles were compared with the Poiseuille solution at an arbitrary instant in the cardiac cycle.

### 2.3.2 Studying the velocity profile development

The development of the profile was studied using the straight pipe model and the two different artificial aneurysm models. The developed profile in the straight tube was compared with the result of the analytic formulae and the development lengths were registered. Varying inlet lengths were applied to the idealised aneurysms (Fig. 1), to check the effects of the non-developed velocity profiles on the flow in the aneurysm sac.

In addition, randomly curved geometries were generated. In the case of bent blood vessels analytical approximation for the velocity distribution is limited to simplified cases [16]. These flows are classified on the basis of the Dean number (Equation (3) [17]).

$$De = \frac{ud}{v} \sqrt{\frac{d}{2C}} \quad (3)$$

Where  $d$  is the diameter of the pipe,  $C$  is the curvature of the pipe section centerline. Since cerebral arteries are curved in a quasi-random way, the following methodology was used. Randomly curved pipe sections were generated. The generating algorithm was such that Dean numbers of the resulting sections were in the same regime than those of the analysed real-life vessel segments. Examples for the resulting curved sections are shown in Fig. 3 along with a reference angiogram image of the cerebral arteries.

The generated curved vessels were then dissected into two parts of equal lengths. In all cases the three geometries (complete, upstream section and downstream section) were equipped with the same boundary conditions and simulated. By comparing the results from the complete and the downstream section geometry it was possible to study the effect of the bends on the inlet profile development. This was done by comparing velocity profiles at the same locations, at a series of planes with a distance of  $5d$  from each other, perpendicular to the vessel axis. The spatial average of the relative error was calculated in all sections which enabled the determination of the profile development length.

The development of the flow in a real geometry with different inlet lengths was studied to check if the findings in the idealised vessel section are valid also in realistic geometries. The mesh of the real geometry was supplemented in order to suit the boundary conditions applied in the case of artificial geometries. Five configurations of different inlet vessel lengths

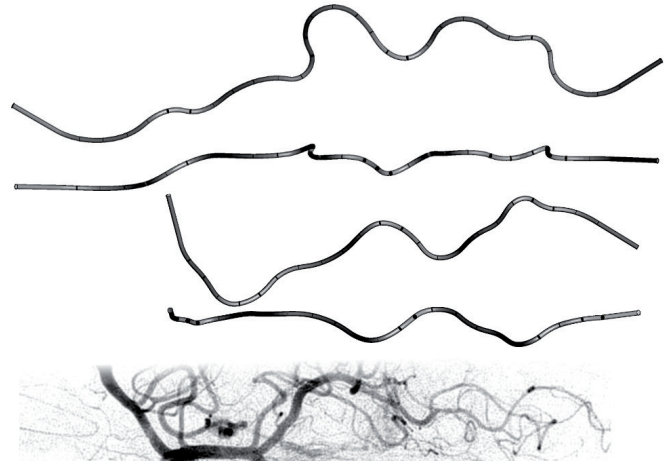


Fig. 3. Two examples of generated curved vessel sections (top and centre) displayed with two views and a reference picture of the arteries in the brain (bottom)

were prepared to study the flow development in a real aneurysm geometry. The first geometry is the base geometry created by removing most of the inlet vessel section. Only an approximately  $2d$  long inlet section remained in this configuration. Additionally, geometries with the inlet section represented by one, one and a half or two bends. Finally, the reference geometry consisting of 7 bent sections on a vessel length of approximately  $25d$ . The resulting flows were compared in terms of velocity and WSS distribution in the base geometry.

## 2.4 Outlet condition studies

A porous media approach was followed at the outlet boundary. The modifying effects of the exiting pipe length were also checked in case of the two idealised aneurysm geometries. The effects of the curved geometry were studied at the outlet boundary condition.

### 2.4.1 Porous medium modelling of the outlet boundary condition

In all cases a  $10d$  long porous pipe section was attached to the outlet region. The porous medium was modelled after Darcy (Eq. (4)).

$$-\frac{\partial p}{\partial x} = \frac{\mu}{K} u + B\rho|u|u \quad (4)$$

Where  $p$  is the pressure,  $\mu$  is the dynamic viscosity,  $K$  is the so-called permeability,  $u$  is the axial velocity,  $B$  is an empirically determinable constant,  $\rho$  is the density and  $x$  is the coordinate in the flow direction. The second term on the right hand side may be neglected here due to low flow velocity. The permeability of the porous domain and the outlet pressure were set so that the mean pressure inside the flow domain remained within the range of the realistic 80 - 120 mmHg [18] induced by the prescribed pulsation of the flow rate (see Fig. 2).

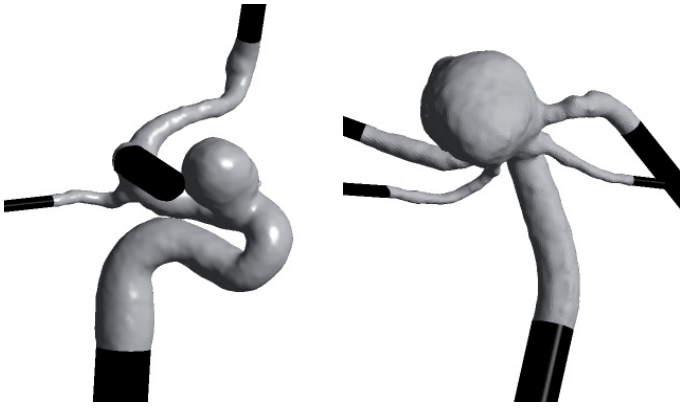


**Fig. 4.** Modified real aneurysm geometries to study the effects of compliant walls after the extrusion (darker areas) of the in- and outlet vessels in case of a side-wall (left) and a bifurcation aneurysm (right)

#### 2.4.2 The effects of the exiting pipe length

To study the effects of various exiting lengths, the two idealised aneurysm models and the randomly curved pipes were used. The complete and the upstream section of the curved pipes were compared. The differences in the flow with varying exit conditions could thus be observed.

### 2.5 Methods involved in compliant wall studies

To model the compliance of the wall, a fully coupled fluid-structure interaction approach was applied. Both artificial aneurysms and the real aneurysm models were included in this study. The resulting velocity, WSS and pressure distributions in the compliant simulations were studied and compared with the corresponding rigid-walled results. The final geometries of the real aneurysm models with extruded boundaries are depicted in Fig. 4.

As far as fluid mechanics is concerned, the boundary conditions were similar to those rigid-walled models. The constraints of the solid body model were the flow-induced wall loads inside and elastic support applied on the outside, and the fixed original vessel ends. The elastic support is needed to avoid unrealistic expansion of the geometry, which may lead to negative element volumes in the CFD mesh rendering it impossible to obtain results. The elastic support is suitable for modelling the resistance against movement of the tissues surrounding the vessels. The modulus for the elastic support was set to zero in case of the artificial geometries and it was set to 96,000 Pa/mm in the case of the real aneurysm models.

## 3 Results

### 3.1 Inlet boundary condition

#### 3.1.1 Analytical studies

With the reconstruction of the Womersley profile the effect of various properties of the cardiac cycle on the flow was studied. These included the temporal mean of the volume flow, the frequency of the beats and the positions of the three characteristic points indicated in Fig. 2. The Poiseuille solution, calcu-

lated from the actual flow rate value, and the exact Womersley solution were compared. The relative error of both the WSS and the spatial peak velocity of the profiles were examined. The comparison is provided with various parameters changing and the maximum differences are indicated throughout a cycle.

The mean value of the flow rate is apparent in the Womersley formulae as the weight factor of its zeroth term (see Eq. (2)), which is the parabolic part of the profile. Thus it is expected that the higher the mean value of the flow rate is, the more the Womersley profile will resemble the steady parabolic solution. By decreasing or increasing the mean value of the flow rate from the reference value in Fig. 2 by 20%, the WSS maximum error changed from 49% to 72% and 39%, respectively. The maximum peak velocity error changed from 15% to 19% by decreasing and 13% by increasing the mean flow rate.

By increasing the frequency of the cycles, the parabolic approximation of the velocity profile becomes less suitable, since the unsteady behaviour of the flow begins to dominate the solution. A 12% change in the beat frequency causes approximately the same change in the maximum WSS error, and 2% change in the maximum error of the spatial velocity peak.

The effect of the magnitude of the characteristic points of a cardiac cycle (Fig. 2) on the velocity profile was also investigated. Out of the two peak flow rates in a typical beat, changing the larger one (systolic peak) has a significantly larger effect. 20% change of the peak volume flow resulted in 20% increase or decrease of the relative WSS error. On the other hand, changes of the errors were not higher than 1% when changing the second peak. The velocity profile was found to be sensitive to the magnitude of the minimum flow rate after the systolic peak. A 20% change caused approximately 17% change in the WSS error and 3% in the spatial peak velocity error.

The phase of the maximum WSS error mostly occurred at the minimum value after the systolic peak. When the systolic peak had a significantly higher slope than that in Fig. 2 the maximum error was shifted before the systolic peak.

A phase shift between the WSS and the velocity cycle was detected which is characteristic of the Womersley solution, the Poiseuille solution stayed in phase. Consequently, the maximum WSS value occurs  $0.054T$  ( $T$  being the time period of the beat) earlier than the maximum velocity in case of the reference beat. The shifted phases of the WSS histories of the Womersley and the Poiseuille solutions are depicted in Fig. 5.

Phase shifting, being a temporal phenomenon, is not sensitive to the changing values of the mean flow rate or the flow rate magnitude of the characteristic points. The frequency of the beats, however, has an influence on the phase shift. A 25% increase or decrease in the period time of the beat results in  $0.049T$  and  $0.063T$  phase shift between the WSS and the velocity (and, therefore, the Poiseuille WSS) maximum value, respectively. The changing shape of the systolic peak also has a significant effect on the phase shift. The tendency is that the

higher the slope of the systolic peak is, the smaller the phase shift becomes relative to the time period of the cycle. This also gives an explanation for the varying phase of the maximum WSS errors.

### 3.1.2 Inlet profile development

The development of the velocity profiles in different geometries was checked. In case of a straight rigid tube it was found that depending on the beat shape, approximately 20 - 30d is the necessary length for a parabolic profile to develop into a perfect Womersley profile (the relative error being within 1%). Idealised aneurysm geometries showed that if the inlet length is 0d and the inlet profile is parabolic at the location of interest there are significant errors (10%) in the flow compared to a 20d long inlet. The error in case of 10d is below 3% in case of the side-wall aneurysm (case a). Even shorter pipe sections were sufficient to capture the velocity distributions accurately in the bifurcation aneurysm (case b) model. Following this finding all studies were carried out using a 10d long pipe section attached to the inlet boundary applying a parabolic velocity distribution at the inlet boundary, whose maximum velocity changes in time following Fig. 2.

The results of curved vessel geometries (Fig. 3) showed that a limited portion of the curved pipe before the investigated section is sufficient for a faithful reproduction of the flow. The effect of the upstream bent sections on the flow decreases as the fluid flows through additional bends of the pipeline. A typical plot of the processed results is shown in Fig. 6.

Here, the comparison between the original curved vessel and both the upstream section and downstream sections is presented, in the respective planes. The highest peak (15<sup>th</sup> plane) appears directly before the transition between the compared parts and is a result of the geometric differences of the original and separated cases.

Regarding the inlet length it can be observed in the right part of Fig. 6 that at the systolic peak following a 20% error at the first matching plane (16<sup>th</sup> plane) it takes five planes (20d) for the error to decrease below an acceptable 5%. This occurs even sooner in case of lower inflow velocities. It was found in all cases that the errors reach an acceptable level after the first bend (corresponds to the 20<sup>th</sup> plane in Fig. 6). The compared velocity magnitude distributions in a plane directly after the first bend are depicted in Fig. 7.

It was also found that although in the intensive flow region the agreement is not perfect at certain areas in the early sections of the truncated curved pipe section, the flow near the wall has a good agreement with the reference simulation in these early parts. This suggests that the WSS errors decrease more rapidly than the velocity errors of the cross sections (Fig. 6). An additional effect is demonstrated in Fig. 6. After a certain length the error increases slightly (25<sup>th</sup> plane) then decreases again. Due to the highly 3D nature of the flow the orientation of the stream is

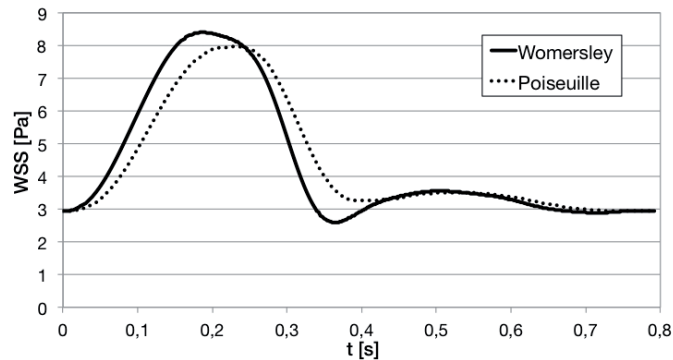


Fig. 5. WSS histories of the Womersley and the Poiseuille solutions, the latter corresponding to the Womersley velocity history

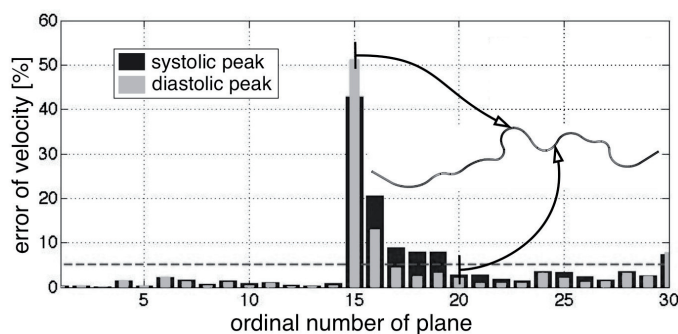


Fig. 6. Typical plot of the average errors of velocity in a curved vessel with different preceding section lengths at two instants of the cardiac cycle

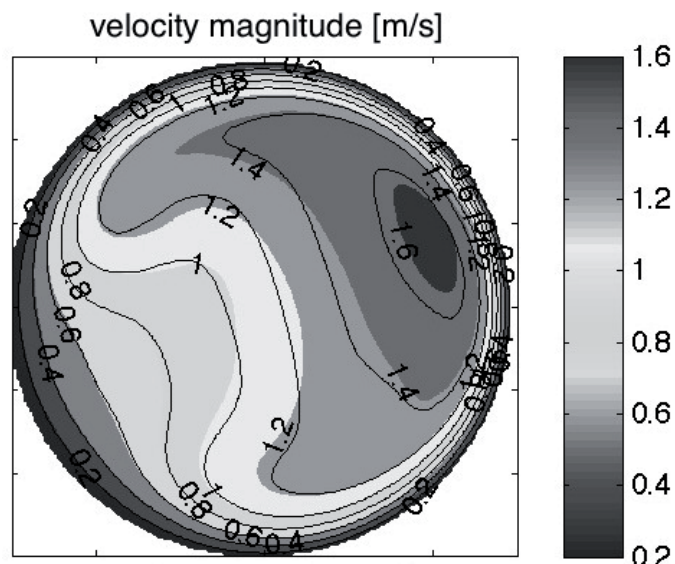
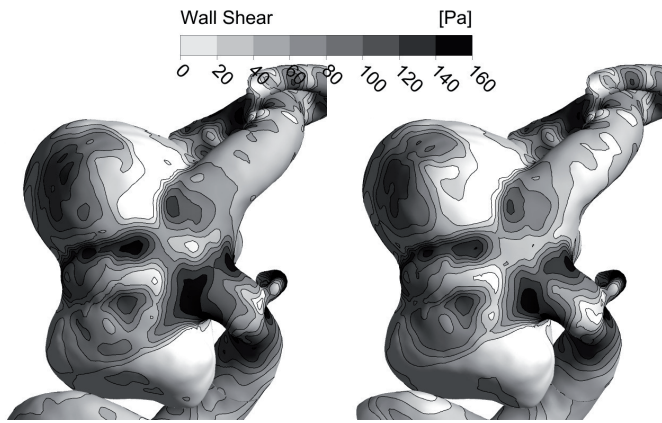


Fig. 7. Compared contour plots of the velocity profile in plane 20 obtained from simulations of the whole bent vessel geometry (filled contour) and the downstream section only (contour lines)



**Fig. 8.** WSS distribution with different curved inlet vessel lengths (reference simulation on the left and one and a half bend on the right side) in a real aneurysm geometry at the systolic peak instant

suspected to change differently than in the reference simulation. This suggests that the effect of a removed bend in a vessel can propagate far, but this appears to be a negligible source of error.

In the real aneurysm geometry a similar behaviour of the flow was found. The velocity distribution in a cross section of the inlet vessel just before entering the aneurysm was compared. The average velocity difference with the reference simulation was found to be 22%, 9%, 6% and 8% in cases with the base geometry, one, one and a half and two bends, respectively, that agrees well with the findings in the artificial geometries. The resulting WSS distribution in case of one and a half bend and the reference simulation is compared in Fig. 8.

The compared WSS distributions show good agreement. The peak values are all located at the same places and the values are almost identical.

### 3.2 Outlet boundary condition

Studying the sufficient exiting pipe length before the porous region, no differences could be found in the velocity distributions with increasing length. In terms of the pressure, only a slight increase in the absolute values was found due to the increased friction loss on the pipe wall. The highest increase occurred in the case of the bifurcation aneurysm model but that was lower than 2%. In case of the curved vessels the same was found. In Fig. 6, before the 15<sup>th</sup> plane no significant differences were found between the upstream section and the whole model in case of the velocity distribution.

### 3.3 Wall compliance findings

Studying the idealised aneurysm geometries with compliant walls revealed that all the basic, hemodynamically relevant flow variables are influenced by the compliant boundaries. Studying the deformation of the geometries it was found that with our assumption of fixed ends the main direction of the geometry movement is the axis of the aneurysm sac.

Additionally to this movement, an expansion of the geometries was found. The highest deformation is located in the vicinity of the aneurysm sac. The upward motion of the aneurysm sac in case a) prevents the intensive direct flow onto the downstream neck section (connection between the pipe and the sac) of the geometries where the highest WSS values are usually located. This causes decreased maximum WSS values. The difference between the peak values in rigid and compliant geometries may reach -52%. The decrease is also apparent in the spatial mean value of WSS; this is 16% on the average. The average velocity magnitude in the flow domain was found to decrease in both cases on average by 12%, but the qualitative appearance of the flow did not change. In case b) the deformation resulted in small flow separation zones without changing the overall quality of the flow.

The pressure level change is influenced by two opposite processes. The expanding geometry reduces the pressure in the volume while the decreased average velocity causes a pressure rise. As a result a 2 - 5% decrease was found with wall deformability in both idealised cases, the decrease is higher at higher volume flow rates.

Studying the realistic models revealed similar findings. Here, the applied elastic support enabled only small deformations. The side-wall aneurysm geometry exhibited a more complex movement, a slight twisting of the aneurysm sac around its axis. No notable changes in the average velocity and pressure have been found due to the small deformation. No qualitative differences have been detected in the velocity distribution. The average wall shear stress values decreased by less than 10% and less than 5% in case of the compliant geometry of the side-wall aneurysm and bifurcation aneurysm, respectively. The peak WSS decrease also remained within 10% in both cases.

## Discussion

In the present paper a study on the boundary conditions of cerebral aneurysm simulations is presented but the results may be applicable in the research of other parts of the circulatory system as well. In all hemodynamic simulations the region of interest has to be “cut out” from the circulatory system and it has to be assumed that the flow conditions there are the same as in the complete system. The boundary conditions given for our isolated system have a decisive influence on the accuracy of the results, therefore, they have to be chosen with particular care. Flow in arteries are internal flows, therefore, the covered topics are the in- and outlet conditions, and the bounding walls.

In case of the inlet boundary conditions, effects of the pulse shape of the cardiac cycle on the velocity profile are discussed. It was found that by increasing the mean volume flow the velocity profile tends to the steady parabolic profile. Increasing frequency acts inversely and magnifies the unsteady part of the solution of the velocity profile. By changing the magnitude of the characteristic points of the beat it was found that the

highest influence of the beat on the flow is due to the change of the systolic peak flow rate, and the second highest influence is due to the change of the minimum flow rate after this peak. The second peak flow rate was found to be unimportant.

The phase shift between the velocity and the wall shear stress (WSS) cycle, which appears as a consequence of the correct reconstruction of the Womersley profile, is dependent on the frequency and the shape of the pulse. The phase shift is typically 5 - 7% of the period. The maximum WSS values occur, therefore, at an earlier instant than the maximum velocity or pressure.

Although some quantitative differences were found in the case of varying beat characteristics, an artificial cardiac cycle may be used in cases when no patient-specific data is available if we have information on the peak flow rate and the following minimum. Cebal et al. [3] found the flow to be insensitive to the varying mean flow rate, apart from some small quantitative changes. Our results imply that the differences between the Poiseuille and Womersley solution become more important in large arteries closer to the heart. Here the pulsation amplitude of the volume flow inside a cycle is more significant, making the Womersley solution dominant. Farther from the heart on the arterial network such as in cerebral arteries the flow has a significant steady part due to the Windkessel mechanism [18]. Our results imply that in these regions the assumption of the parabolic velocity distribution is a permissible approximation.

Profile development studies showed that a 10d long straight pipe is sufficient for the development of the Womersley solution if the prescribed velocity profile was parabolic with the maximum velocity varying according to the cardiac cycle. This allows the phase shifting phenomenon of the Womersley solution to be taken into account in the simulations. The curved pipe studies imply that after the first bend the effects of most previous bends on the flow is dominated by the new geometrical conditions. Oshima et al. [19] demonstrated the sensitivity

of the flow inside the aneurysm sac to secondary flow at the inlet boundary. Castro et al. [14] found that neglecting the parent artery leads to significant differences in the intra-aneurysmal flow. They concluded that individual sensitivity analyses are necessary for all typical aneurysm locations to determine the necessary inlet length. Our results agree with these findings and provide the first estimate of a universal criterion for accurate results. The study featuring a real aneurysm geometry confirms the findings in artificial geometries.

Investigations of the outlet length showed that in simple cases, the outlet condition has only a localised effect on the flow pattern.

The study on compliant boundaries showed that all main hemodynamic variables might be influenced when the movement of the boundary is taken into account. The highest differences were found for the wall shear stress. In the basic flow pattern no strong qualitative changes occurred, although in case of the idealised bifurcation aneurysm model small separation zones appeared. The pressure decreased slightly in the studied flows (less than 5%). These findings indicate that strictly speaking compliant boundaries are needed for the correct estimation of the wall shear stress magnitudes. This is in accordance with Torii et al. [12] and Dempere-Marco et al. [20], who found that simulations with rigid walls tend to overestimate the WSS compared to distensible boundaries. Nevertheless, the computational effort to perform compliant simulations exceeds significantly the effort needed for rigid-walled simulations. To model the wall movement accurately, several physical parameters are needed in connection with the wall and its environment. In the absence of these our results suggest that simulations with rigid walls are still able to deliver qualitatively correct results. Specifically, when large number of simulations are needed for qualitative parametric studies, the rigid-walled simulations yield qualitatively correct results and thus their usage is justified.

## Acknowledgements

This work has been supported by the "Öveges József" PhD scholarship of GE Hungary ZRt. Healthcare Division.

This work is related to the scientific program of the "Development of quality-oriented and harmonized R+D+I strategy and functional model at BME" project. This project is supported by the New Széchenyi Plan (Project ID: TÁMOP-4.2.1/B-09/1/KMR-2010-0002 ).

## References

- 1 Ecker R. D., Hopkins L. N., *Natural history of unruptured intracranial aneurysms*. Neurosurgical Focus, 17(5), 1-5 (2004).
- 2 Sforza D. M., Putman C. M., Cebal J. R., *Hemodynamics of cerebral aneurysms*. Annual Review of Fluid Mechanics, 41(1), 91-107 (2009).  
DOI: [10.1146/annurev.fluid.40.111406.102126](https://doi.org/10.1146/annurev.fluid.40.111406.102126)
- 3 Cebal J. R., Castro M. A., Appanaboyina S., Putman C. M., Millan D., Frangi A. F., *Efficient pipeline for image-based patient-specific analysis of cerebral aneurysm hemodynamics: Technique and sensitivity*. IEEE Transactions on Medical Imaging, 24(4), 457-467 (2005).  
DOI: [10.1109/TMI.2005.844159](https://doi.org/10.1109/TMI.2005.844159)
- 4 Shojima M., Oshima M., Takagi K., Torii R., Hayakawa M., Katada K., Morita A., Kirino T., *Magnitude and role of wall shear stress on cerebral aneurysm: Computational fluid dynamic study of 20 middle cerebral artery aneurysms*. Stroke, 35(11), 2500-2505 (2004).  
DOI: [10.1161/01.STR.0000144648.89172.0f](https://doi.org/10.1161/01.STR.0000144648.89172.0f)
- 5 Castro M. A., Putman C. M., Cebal J. R., *Patient-specific computational fluid dynamics modeling of anterior communicating artery aneurysms: A study of the sensitivity of intra-aneurysmal flow patterns to flow conditions in the carotid arteries*. American Journal of Neuroradiology, 27(10), 2061-2068 (2006).

- 6 Paal G., Ugron A., Szikora I., Bojtar I., *Flow in simplified and real models of intracranial aneurysms*. International Journal of Heat and Fluid Flow, 28(4), 653-664 (2007).  
DOI: [10.1016/j.ijheatfluidflow.2007.04.004](https://doi.org/10.1016/j.ijheatfluidflow.2007.04.004)
- 7 Formaggia L., Nobile F., Quarteroni A., Veneziani A., *Multi-scale modelling of the circulatory system: a preliminary analysis*. Computing and Visualization in Science, 2, 75-83 (1999).  
DOI: [10.1007/s007910050030](https://doi.org/10.1007/s007910050030)
- 8 Nicoud F., Schönfeld T., *Integral boundary conditions for unsteady biomedical cfd applications*. International Journal for Numerical Methods in Fluids, 40(3-4), 457-465 (2002).  
DOI: [10.1002/flid.299](https://doi.org/10.1002/flid.299)
- 9 Zamir M., *The Physics of Pulsatile Flow*. Springer (2000).
- 10 Cebal J. R., Castro M. A., Soto O., Löhner R., Alperin N., *Blood-flow models of the circle of willis from magnetic resonance data*. Journal of Engineering Mathematics, 47, 369-386 (2003).  
DOI: [10.1023/B:ENGI.0000007977.02652.02](https://doi.org/10.1023/B:ENGI.0000007977.02652.02)
- 11 Grinberg L., Karniadakis G., *Outflow boundary conditions for arterial networks with multiple outlets*. Annals of Biomedical Engineering, 36(9), 1496-1514 (2008).  
DOI: [10.1007/s10439-008-9527-7](https://doi.org/10.1007/s10439-008-9527-7)
- 12 Torii R., Oshima M., Kobayashi T., Takagi K., Tezduyar T. E., *Influence of wall elasticity in patient-specific hemodynamic simulations*. Computers and Fluids, 36(1), 160-168 (2007).  
DOI: [10.1016/j.compfluid.2005.07.014](https://doi.org/10.1016/j.compfluid.2005.07.014)
- 13 Venugopal P., Valentino D., Schmitt H., Villablanca J. P., Vinuela F., Duckwiler G., *Sensitivity of patient-specific numerical simulation of cerebral aneurysm hemodynamics to inflow boundary conditions*. Journal of Neurosurgery, 106(6), 1051-1060 (2007).  
DOI: [10.3171/jns.2007.106.6.1051](https://doi.org/10.3171/jns.2007.106.6.1051)
- 14 Castro M. A., Putman C. M., Cebal J. R., *Computational fluid dynamics modeling of intracranial aneurysms: Effects of parent artery segmentation on intra-aneurysmal hemodynamics*. American Journal of Neuroradiology, 27(8), 1703-1709 (2006).
- 15 Womersley J. R., *Method for the calculation of velocity, rate of flow and viscous drag in arteries when the pressure gradient is known*. The Journal of Physiology, 127(3), 553-563 (1955).
- 16 Pedley T. J., *The Fluid Mechanics of Large Blood Vessels*. Cambridge University Press, (1980).  
DOI: [10.1017/CBO9780511896996](https://doi.org/10.1017/CBO9780511896996)
- 17 Ku D. N., *Blood flow in arteries*. Annual Review of Fluid Mechanics, 29, 399-434 (1997).  
DOI: [10.1146/annurev.fluid.29.1.399](https://doi.org/10.1146/annurev.fluid.29.1.399)
- 18 Nichols W. W., O'Rourke M. F., *McDonald's Blood Flow in Arteries: Theoretical, Experimental and Clinical Principles*. 5<sup>th</sup> ed., Oxford University Press (2005).
- 19 Oshima M., Sakai H., Torii R., *Modelling of inflow boundary conditions for image-based simulation of cerebrovascular flow*. International Journal for Numerical Methods in Fluids, 47(6-7), 603-617 (2005).  
DOI: [10.1002/flid.834](https://doi.org/10.1002/flid.834)
- 20 Dempere-Marco L., Oubel E., Castro M. A., Putman C. M., Frangi A. F., Cebal J. R., *CFD analysis incorporating the influence of wall motion: Application to intracranial aneurysms*. in 'Medical Image Computing and Computer-Assisted Intervention – MICCAI 2006. (eds.: Larsen R., Nielsen M., Sporring J.), Proceedings 9th International Conference, Copenhagen, Denmark' Series: Lecture Notes in Computer Science, Vol. 4191, 438-445 (2006).